HI Narrow Line Absorption in Dark Clouds

D. Li[1,2] and P. F. Goldsmith[2]

ABSTRACT

We have used the Arecibo telescope to carry out an unbiased survey of 31 dark clouds in the Taurus/Perseus region for narrow absorption features in HI (λ 21cm) and OH (1667 and 1665 MHz) emission. We detected HI narrow line absorption (HINLA) in about 80% of the clouds that we observed. HINLA and OH emission, observed simultaneously are remarkably well correlated. Spectrally, they have the same nonthermal line width and the same peak velocity. Spatially, they both peak at the optically–selected central position of each cloud, and both fall off toward the cloud edges. Sources with clear HINLA feature have also been observed in transitions of CO, ^{13}CO, C^{18}O, and CI. HINLA exhibits better correlation with molecular tracers than with CI.

The line width of the absorption feature, together with analyses of the relevant radiative transfer provide upper limits to the kinetic temperature of the gas producing the HINLA. Some sources must have a temperature close to or lower than 10 K. The correlation of column densities and line widths of HINLA with those characteristics of molecular tracers suggest that a significant fraction of the atomic hydrogen is located in the cold, well–shielded portions of molecular clouds, and is mixed with the molecular gas.

The average number density ratio [HI]/[H_2] is 1.5×10^{-3}. The inferred HI density appears consistent with but is slightly higher than the value expected in steady state equilibrium between formation of HI via cosmic ray destruction of H_2 and destruction via formation of H_2 on grain surfaces. The distribution and abundance of atomic hydrogen in molecular clouds could be critical tests of dark cloud chemistry and structure, including issues of grain surface rates, PDRs, circulation, and turbulent diffusion. The HINLA would appear to have great importance as well as a possible tracer of magnetic fields in dark clouds.

Subject headings: ISM: atoms – individual (hydrogen)

---

[1]Center for Astrophysics, 60 Garden Street, Cambridge MA 02138, dli@cfa.harvard.edu

[2]National Astronomy and Ionosphere Center, Department of Astronomy, Cornell University, Ithaca NY 14853

1. INTRODUCTION

Two relatively distinct phases are generally assumed to exist in the neutral interstellar medium (ISM): atomic and molecular. The atomic phase of the ISM, consisting mainly of hydrogen atoms, is traced by the HI hyperfine transition at λ 21cm. The molecular phase of the ISM, whose major component – molecular hydrogen – lacks a permanent electric dipole moment and readily excited transitions at temperatures generally encountered, is primarily traced by emission from rarer molecular species such as carbon monoxide. The conversion from atomic to molecular forms occurs on dust grains, where atomic hydrogen sticks and forms H_2. This exothermic reaction releases H_2 into the gas and keeps molecular clouds molecular. Dissociative processes, however, will maintain a population of atoms even inside molecular clouds. Recently, there has been increased interest in atomic species, which prove to be important probes. Two important examples are CI, which is now accessible at submillimeter wavelengths (**?**, e.g.)]plume00, and OI, which can be observed in the far infrared (**?**, e.g.)]herr97, kram98, lise99, lis01.

Inside molecular clouds, dissociating UV photons are blocked both by grains and by H_2 line absorption (Hollenbach, Werner, & Salpeter 1971). A significant HI population, however, exists inside molecular clouds maintained by cosmic ray destruction of H_2 and additionally as a remnant of the H_2 formation process in a chemically young cloud. This atomic component inside molecular clouds has fractional abundance ([H]/[H_2]) of more than 0.1% (Table 3) and is thus the third most abundant gas phase species, after H_2 and He. Because the balance of HI and H_2 involves grain surface reactions, the density of atomic HI in dark clouds could be a test of complete chemical networks with reactions both in the gas phase and on grain surfaces. The HI abundance in well–shielded regions can be increased by relatively rapid turbulent diffusion (Willacy, Langer & Allen 2002), or by general mass circulation (Chièze & Pineau des Forêts 1989). It is therefore important to establish the presence of HI in the molecular ISM and to determine accurately its abundance.

A unique probe of this component is HI narrow line (which we define to be restricted to $\Delta V < 2$ km s^{-1}) absorption, which we denote HINLA. The absorption dips seen in the spectra of λ 21cm emission in the directions of nearby Galactic dark clouds are often denoted HI self–absorption. The prefix 'self' is widely used to differentiate this phenomenon from absorption against a background continuum source. In terms of its physical origin, *separate* galactic background HI emission and cold foreground HI material are both needed to generate the "self–absorption". A typical configuration is shown in Figure 1. The terminology may be considered somewhat confusing as the absorbing and emitting regions are quite distinct: both do contain atomic hydrogen but under very different conditions. We thus propose the expression HINLA as an alternative term where appropriate.

The existence of cold HI associated with dark clouds was recognized more than 25 years ago. Knapp (1974) conducted a survey of 88 dark clouds and detected HINLA in fewer than half of them. The optical depth of cold HI was derived from the profiles of the absorption lines. The molecular content of the clouds observed was traced by their dust extinction. The HI fractional abundance, $[H]/[H_2]$ was thus determined to be 1% to 5%. In terms of the observational limits and conclusions, this early work typifies most self–absorption studies that have followed.

With the 140ft (43m) telescope, Knapp's survey has an angular resolution of $21'$ and a velocity resolution of $\sim$0.5 km s^{-1}. Similar resolutions have been achieved with the 120ft (37 m) antenna of the Haystack Observatory (Myers et al. 1978). The 76m Lovell telescope ($12'$ angular resolution, $\sim$0.5 km s^{-1} velocity resolution; the same convention in what follows) has been employed for a study of six dark clouds in the Lynds (1962) catalogue (McCutcheon, Shuter & Booth 1978) and the Riegel–Crutcher cloud (Montgomery, Bates & Daves 1995). Additional studies have been conducted with the Effelsberg 100m telescope ($9'$, 0.5 km s^{-1}). The Taurus molecular cloud TMC1 has been mapped by Wilson and Minn (1977). The complex region around B18, also known as Kutner's cloud and Kh 279 (Khavtassi 1960), has been mapped by Batrla, Wilson & Rache (1981) and by Pöppel, Rohlfs & Celnik (1983). The Arecibo telescope with the line feed system ($3'$, 0.5 km s^{-1}) has been used to study HI absorption, with one of the earliest studies being by Baker & Burton (1979). These authors also raise the possibility that the absorption can help resolve the near–far ambiguity in kinematic distances, a topic which is further explored by Jackson et al. (2002).

Interferometers have also been used to obtain higher angular resolution, but the usual penalty has been lower velocity resolution to augment the sensitivity. Van der Werf et al. mapped L134 (1988) and L1551 (1989) with the DRAO and the VLA ($1.5'$, 1.3 km s^{-1}). Similar setups of the DRAO were used in the detailed studies of B5 by Wannier et al. (1992, 1993). The interferometer studies are well–suited for mapping structures having a scale of arc–minutes. But their velocity resolutions of about 1.5 km s^{-1} can easily miss or suppress narrow absorption features, which occupy at most a couple of velocity channels in such spectra. To compound this problem, the HI emission is structured. Multiple peaks and wide troughs are not rare in galactic 21c profiles (see, e.g. Figure 4). If a map is based on the integrated area of an absorption line (or lines), the wide troughs which may not be associated with dark clouds will be more prominent than are the narrow features. Reliable analysis of HINLA profile requires a velocity resolution better than 0.4 km s^{-1}.

The general scientific objectives of narrow line HI absorption studies are to explain its origin and to determine the abundance of atomic hydrogen. For the first question, the association of HINLA with dark clouds is inconclusive in the literature. On the positive side,

Sherwood & Wilson (1981) find a good correlation with extinction in TMC1. McCutcheon et al. (1978) give a higher detection rate (6–8 out of 11 Lynds clouds) than Knapp (1974). Nicolau & Pöppel (1991) find HINLA in the 'darkest' cores in the CrA complex embedded in a HI emission ridge. On the other hand, the association between HI absorption features and dense regions is ambiguous in a recent DRAO HI survey, in which Gibson et al. (2000) find cloud–like absorption structures both correlated and uncorrelated with CO emission. They label these features HISA, shorthand for HI self–absorption. This is the situation in which the distinction between HISA and HINLA must be made. As seen in the DRAO survey, the HISA probably reflects temperature fluctuations in the atomic ISM. The HISA is spectrally wider and flatter and could have its origin in the same location as the 21cm emitting gas, making its name appropriate. HINLA refers to narrower absorption features, which are produced by cold foreground molecular clouds and which are not prominent in the DRAO survey with 1.3 km s^{-1} velocity resolution. To further complicate the issue, HI has also been seen in *emission* in possible halos around molecular clouds, such as B5 (Wannier, Lichten, Andersson, & Morris 1991). HI halos are a distinct environment for atomic hydrogen compared to either HISA or HINLA, and they are easily distinguished observationally (see Section 7).

The difficulties in obtaining the HI abundance through HINLA are three–fold. First, the early studies are hampered mainly by limited knowledge of the dark cloud itself. The H_2 column density is often obtained from low angular resolution extinction data (e.g. Knapp 1973, Batrla et al. 1981) or H_2CO (e.g. Wilson & Minn 1977, Pöppel et al. 1983), a molecule whose fractional abundance is not very certain. Second, with one profile, it is impossible to obtain both the optical depth and the spin temperature accurately. An assumption about the spin temperature is often made, which may not be realistic. Third, the issue of foreground emission is often ignored. With some or all of the three uncertainties, the $[H]/[H_2]$ ratio has been derived in a variety of environments ranging from a few percent (e.g. Knapp 1974; Saito, Ohtani & Tomita 1981), $\sim 10^{-3}$ in M17 (Sato & Fukui 1978), to 5×10^{-4} (Winnberg et al. 1980) in dark clouds.

The requirements of reasonable angular resolution, good sensitivity, and high frequency resolution make the upgraded Arecibo Gregorian system a valuable tool with which to study the HINLA. The large instantaneous bandwidth allows OH 1665 and 1667 MHz spectra to be obtained simultaneously with that of HI. We describe the new observations including a HI survey to examine the correlation between HINLA and OH in dark clouds and complementary mapping in carbon monoxide isotopologues, OH, and CI in Section 2. In Section 3 we present a three–component model for radiative transfer and correction for foreground material, allowing accurate HI column densities to be obtained. We analyze OH and $C^{18}O$ emission in Section 4, and the results of our survey and observation of L1544 in Section 5.

We review the general issue of atomic hydrogen in molecular clouds in Section 6, discuss our results in Section 7, and summarize our conclusions in Section 8.

2. Observations

The sources included in our survey of HI in dark cloud cores are mainly chosen from a dark cloud catalogue based solely on optical obscuration (Lee & Myers 1999). The observed cores meet the following constraints: (1) Right Ascension 2h – 6h, (2) angular diameter close to or larger than $3'$, (3) declination angle 0° – 35°, (4) other observing considerations, such as minimizing slew time. Twenty nine cores have thus been chosen for this Arecibo survey of dark clouds Their names, coordinates, presence of HINLA, and association with a young stellar object are given in Table 1. In addition, two well studied dark clouds in Perseus, Barnard 1 (B1) and Barnard 5 (B5), are included in our survey. B1 is one of the few dark clouds with a positive Zeeman detection (Goodman et al. 1989). The physical conditions of B5 have been well determined through mapping of CO and its isotopologues (Young et al. 1982). The inclusion of these two sources also extends the length of the nightly observing session at Arecibo, due to their early rise times. Because there is no a priori knowledge regarding the HINLA properties of B1 and B5, they should not bias our study of the correlation between HINLA and dark clouds. TMC1 is a well studied region with both strong OH emission and HI absorption. We observe TMC1CP, the cyanopolyyne peak of TMC1 (Pratap et al. 1997), as a secondary calibrator source to check the consistency of data taken at different times. Because it is a previously known strong HINLA source (Wilson & Minn 1977), TMC1CP is excluded from source statistics presented later. In summary, our sample has 31 unbiased sources plus TMC1CP as a calibrator.

L–band observations of nearby dark clouds were conducted at Arecibo in September 1999, February 2001 and January 2002. The $3'$ beam size corresponds to about 0.13 pc at the 140 pc distance of the Taurus dark cloud complex. Most individual nearby clouds fill the main beam at this frequency. The Arecibo spectral line correlator is configured to observe HI and OH (1665 MHz and 1667 MHz) simultaneously. The two lines of OH and the 21cm line of HI are recorded with a channel width of 0.382 kHz, which after smoothing yields a velocity resolution of 0.14 km s^{-1} for OH and 0.16 km s^{-1} for HI. The remaining section of the correlator is employed to record the HI profile at a lower resolution with a wider bandwidth. This is necessary for obtaining a good spectral baseline when the HI emission toward some sources is nearly as wide as the bandpass at the higher resolution, as does occur for some sources (e.g. L1578–2).

The data were taken in a total power (ON scan only) observing mode. The prevalence

of background HI emission and its variation on an arc–minute scale make finding clean OFF positions very questionable. Especially in regions of extended emission, such as the Taurus dark cloud complex, the use of an OFF position can lead to large uncertainties caused by variation in the emission. Sources such as CB 37, shown in Figure 5, illustrate such fluctuations across the band with amplitude comparable to the narrow absorption feature. In a study of HI envelopes, Wannier et al. (1983) find in their sample that the average variation of HI emission across a cloud boundary is 10.9 K at the molecular emission velocity. Fortunately, the narrowness of the absorption dip of interest, together with the stability of the Arecibo system, makes possible the measurement of the line profile even without an OFF scan (see Section 3). In addition to the reduction in the uncertainty due to emission in the OFF scan, the stability of the system also allows a factor of 2 reduction in the statistical fluctuations by eliminating any switching.

The correction for the elevation dependence of the antenna gain and the absolute calibration are carried out by observations of quasars. By cross–scanning these strong point sources, beam maps are also obtained to measure the size of the main beam. In all the data reduction which follows, we treat the slightly elliptical beam to be a circular one with the same solid angle. The derived aperture efficiency is 64% and the main beam efficiency 60%. All L–band data are corrected for the main beam efficiency. This is exact if the source just fills the main beam, and appears to be close to an optimum strategy for an one–parameter calculation (see the Appendix for a detailed discussion of antenna efficiencies and error made in deriving column densities).

Each ON source position was observed for an integration time of 5 to 10 minutes. At the current sensitivity of Arecibo ($T_{sys} \sim 35$ K), Galactic HI profiles without ambiguity caused by noise can be obtained in an even shorter time. The RMS noise level of less than 0.1 K in all our spectra is set by requirement of detecting OH lines, which typically have antenna temperatures in the range of 0.5 K to 1 K. The beam efficiency for data taken in Feb 2001 is significantly higher than it was previously, as a result of surface readjustment for the primary. Relative calibration and consistency checks are carried out using the strongest source, TMC1CP, which was observed both before and after the surface readjustment. The data from 2001 observations were scaled to those obtained at the earlier epoch, when extensive quasar calibration observations were made.

To determine the H_2 column density reliably, $C^{18}O$ data on cores with clear HINLA were obtained in October 2000 at the Five College Radio Observatory (FCRAO). The 'footprint' size of the 16 element SEQUOIA focal plane array is $5.9' \times 5.9'$, which can be smoothed to simulate one Arecibo beam. The data are corrected for the main beam efficiency to give the best estimate of the total mass in the beam as discussed above. By combining $C^{18}O$ and HI

data, the abundance [H]/[H_2] can be obtained. At FCRAO, CO and ^{13}CO spectra were also obtained for comparison with HI absorption line profiles.

The 492 GHz ground state fine–structure line of atomic carbon (CI) has also been observed by the Submillimeter Wave Astronomy Satellite (SWAS) toward clouds with clear HINLA features. As a PDR tracer, CI should be abundant only in low extinction regions. We compare its line characteristics to those of HINLA to examine the importance of photodissociation in maintaining populations of low temperature HI.

3. Three–component Radiative Transfer and Foreground Correction

An absorption spectrum is unique in that both the emitting and the absorbing components are visible in a single profile. The standard approach of analyzing absorption is to reconstruct the emission spectrum from observing one or multiple 'OFF' positions, where the absorption is absent. As noted in section 2,identifying such OFF positions is problematic for HINLA. However, the emission spectrum can still be estimated for HINLA because the absorption line is much narrower (typically a factor of 20) than the background emission. The reconstruction is carried out by fitting a polynomial across the frequencies affected by the absorption in the HINLA spectrum to define the profile that would be present if there were no absorption present. Such a fit works well when the absorption dip is on the side of the emission. When the dip is at the center of the emission, the temperature of the fitted background can be in error by a couple of degrees due to fundamental uncertainty in the shape of the emission spectrum. Fortunately, the optical depth, i.e. the column density, of the absorbing HI thus derived will be affected to a lesser extent because the estimated depth of the absorption is also in error by the same amount (see discussion later in this section).

The classical problem of deriving two quantities, the optical depth and the excitation temperature from one profile is compounded by the possible foreground contamination, which adds more unknowns to the mix. A careful look at the radiative transfer is necessary before any quantitative analysis of the HINLA can be carried out with confidence.

A three–component model is outlined in Figure 1. It represents a general view of the HI absorption in the galaxy. The parameters are defined as

- T_b: background HI temperature ,
- T_f: foreground HI temperature,
- τ_b: background HI optical depth ,

- τ_f: foreground HI optical depth,
- T_x: excitation temperature of HI in the dark cloud ,
- τ: optical depth of HI in the dark cloud,
- T_c: continuum temperature, including the cosmic background and Galactic background emission.

The Galactic background emission is estimated to be about 0.8 K by extrapolating the standard interstellar radiation field (ISRF) to L–band (**?**, e.g.)]win80. $T_c = 3.5$ K is thus used in the analysis which follows.

The raw antenna temperature produced by the three–component system is

$$T_A = [T_b(1 - e^{-\tau_b}) + T_c e^{-\tau_b}]e^{-\tau} e^{-\tau_f} + T_x(1 - e^{-\tau})e^{-\tau_f} + T_f(1 - e^{-\tau_f}) \ . \tag{1}$$

In practice, the final data product, T_R (sometimes called the reported antenna temperature), depends on how the baseline is removed. Since the background continuum is flat across the band in our observations, it will be removed along with the bandpass shape through the baseline fitting procedure. Thus,

$$\begin{aligned} T_R &= T_A - T_c \\ &= T_b(1 - e^{-\tau_b})e^{-\tau} e^{-\tau_f} + T_x(1 - e^{-\tau})e^{-\tau_f} + T_f(1 - e^{-\tau_f}) + T_c(e^{-\tau} e^{-\tau_b} e^{-\tau_f} - 1). \end{aligned} \tag{2}$$

Another quantity is derived from the spectrum by fitting a polynomial to the portion of the spectrum without the absorption. We call this quantity T_{HI}, which is the HI temperature that would be observed if there were no absorbing cold cloud

$$T_{HI} = (T_h - T_c)(1 - e^{-\tau_h}) \ , \tag{3}$$

where we have defined the total optical depth from foreground plus background hydrogen to be

$$\tau_h = \tau_f + \tau_b \ , \tag{4}$$

and we have assumed the background and foreground HI to be at the same temperature, viz.

$$T_h = T_b = T_f \ . \tag{5}$$

To consolidate the variables, we define

$$\tau_b = p\tau_h \ , \tag{6}$$

where p can be calculated from a local HI distribution model. To first order, the Galactic HI disk can be approximated by a single Gaussian with a full width half maximum (FWHM) vertical extent z equal to 360 pc (Lockman 1984). The percentage of HI emission in the background is thus given by the complementary error function

$$p = erfc[\sqrt{4\ln(2)}D\sin(b)/z] \ , \tag{7}$$

where D is the distance to the absorbing cloud, b is its galactic latitude, and $erfc(x) = 1 - \frac{2}{\sqrt{\pi}}\int_0^x e^{-t^2}dt$. Taking the difference of T_{HI} and T_R, we can obtain, as a positive quantity, the absorption temperature

$$\begin{aligned} T_{ab} &= T_{HI} - T_R \\ &= (T_c - T_h)e^{-\tau_h} + (T_h - T_x)e^{-\tau_f} + (T_h - T_c)e^{-(\tau+\tau_h)} + (T_x - T_h)e^{-(\tau+\tau_f)} \\ &= [(T_c - T_h)e^{-\tau_h} + (T_h - T_x)e^{-\tau_f}](1 - e^{-\tau}) \ . \end{aligned} \tag{8}$$

Thus, the problem reduces to two equations (3 & 8) and three unknowns (T_h, τ_h & τ). For the Cold Neutral Medium (CNM), which is responsible for most of the 21cm emission here, T_h can be taken to have an average value of 80 K. Thus, in principle, we can solve for τ_h assuming uniform T_h (along with other, less critical assumptions). In the following limiting cases, we develop a recipe for analyzing the absorption spectrum without requiring any assumption about the HI temperature.

Without foreground, the absorption temperature becomes

$$T_{ab} = [T_b(1 - e^{-\tau_b}) + T_c e^{-\tau_b} - T_x](1 - e^{-\tau}) \ . \tag{9}$$

Variations of equation (9) have been employed in the past studies. Usually, spectra of OFF positions have to be used to try to eliminate T_b and T_c.

Our approach requires only ON spectra and recognizes that

$$T_{ab} = [T_{HI} + T_c - T_x](1 - e^{-\tau}) \ , \tag{10}$$

where equation (3) is already incorporated and T_{HI} is derived from a fit to the emission part of the spectrum [3]. The remaining unknowns in the equation above are only τ and T_x.

[3]This demonstrates that we can think of the absorption having optical depth τ taking place against an emitting cloud at a temperature equal to $(T_{HI} + T_c - T_x)$.

The excitation temperature of the 21cm line in dark clouds is determined by the balance between collisions and spontaneous emission. Radiative trapping is unlikely to be significant as optical depths are not significantly in excess of unity. The radiation field is essentially that only of the Galactic continuum plus the cosmic background. As a result of the very small value of $h\nu/kT_c = 0.068/T_c$ (where T_c is the effective temperature of the radiation field ~ 3.5 K, as mentioned above), stimulated emission can be neglected relative to spontaneous emission in the analysis of excitation. The solution to the two level problem is given by Purcell & Field (1956) as

$$T_s = \frac{y}{1+y}T_k + \frac{1}{1+y}T_c \ , \tag{11}$$

where T_s is the spin temperature (the excitation temperature T_x in our terminology), T_k is the kinetic temperature of the gas in the dark cloud, and T_c is the effective radiation temperature. The quantity y is defined by

$$y = \frac{h\nu}{kT_k}\frac{C_{ul}}{A_{ul}} \ , \tag{12}$$

where C_{ul} is the collisional deexcitation rate and A_{ul} is the spontaneous decay rate, 2.85×10^{-15} s^{-1} (Wild 1952). There have been various calculations of the collision rates for the deexcitation of the 21cm line, but the most relevant are the spin–exchange collisions with another hydrogen atom (Field 1958; Allison & Dalgarno 1969). The collisional deexcitation rates calculated with a full quantum scattering code in the latter reference are considerably smaller than values determined earlier, and for a temperature $T_k = 10$ K yield a value y = $5.5n_1$, where n_1 is the atomic hydrogen density in cm^{-3}.

For y >> 1, the excitation temperature approaches the kinetic temperature of the gas. This requires an atomic hydrogen density of at least 1 cm^{-3}. As we show in the following, this is a reasonable value for atomic hydrogen density. Inside dark clouds, most of the hydrogen is in the form of molecules. But as discussed in Section 6, a steady state HI density can be maintained by cosmic ray destruction of H_2; this density is independent of the density of H_2. The standard model gives $n_1 \sim 1$ cm^{-3}, in reasonable agreement with our observations. Thus, the assumption of thermalization is justified. For lower densities, since T_c is less than T_k, the excitation temperature will be below the kinetic temperature.

With the knowledge of T_k obtained from molecular tracers such as NH_3 and CO, the optical depth of the absorption feature can be derived from equation (10), and the column density of atomic hydrogen is given by

$$\frac{N(\mathrm{HINLA})}{\mathrm{cm}^{-2}} = 1.95 \times 10^{18} \tau_0 \frac{\Delta V}{\mathrm{km\ s}^{-1}} \frac{T_k}{\mathrm{K}} \ , \tag{13}$$

where τ_0 is the peak optical depth and ΔV is the FWHM of the absorption line (a Gaussian line profile has been assumed).

Now let us consider the effect of optically thin foreground and background HI. Equation 8 can be written in this situation as

$$T_{ab} = [pT_{HI} + T_c - T_x + (T_x - T_c)\tau_f](1 - e^{-\tau}) \ . \tag{14}$$

Compared to equation (10), the differences are the factor p and the term $(T_x - T_c)\tau_f$. In the HINLA scenario, $(1-p)T_{HI}$ is always greater than $(T_x - T_c)\tau_f$. This means that the absorption dip is partially filled in by the foreground emission, i.e. T_{ab} appears to be smaller.

The major source of uncertainty lies in the estimate of p. Although models of a Gaussian disk are generally accepted, (e.g. Lockman 1984 and Burton 1988), separate evidence indicates that a HI deficiency exists in the solar neighborhood (e.g. Kulkarni & Heiles 1988) and that a larger portion of HI clouds than that predicted by the Gaussian disk model exist at high $|z|$ (Hobbs et al. 1982). Both complications will make the p derived from the single Gaussian an underestimate, i.e., exaggerate the effect of foreground filling of the absorption dip. The magnitudes of these and other uncertainties related to p are examined by comparing results derived both with and without the foreground correction. The fractional uncertainties are generally less than 30% in our sample.

The limiting case described by equation (14) is valid for the objects in this study. The HI foreground of nearby and low galactic attitude dark clouds is optically thin. Based on the HI emission toward positions in our list, the background HI optical depth (τ_b) ranges between 0.3 and 1, assuming $T_b = 80$ K. Note that this provides a rough estimate of the small term $(T_x - T_c)\tau_f$ to be less than 1.3 K. It is indeed small compared to $pT_{HI} \simeq 60$ K under the same assumptions and is ignored in what follows.

In summary, the recipe we have used for obtaining the HINLA column density involves, first, fitting the emission line profile to determine T_{HI}, second, using a model of Galactic HI to determine p, third, deriving the peak optical depth of the cold HI through

$$\tau_0 = \ln(\frac{pT_{HI} + T_c - T_x}{pT_{HI} + T_c - T_x - T_{ab}}) \ , \tag{15}$$

with the kinetic temperature assumed to be 10 K based on measurements of CO and other tracers of dark clouds. Fourth, we use equation (13) with the line width fitted to the absorption feature, to determine the column density. The intrinsic uncertainty comes primarily from three aspects of the recipe. The HINLA opacity is likely to be overestimated by up to 30% due to the imperfect knowledge of the Galactic HI disk. The $(T_x - T_c)\tau_f$ term is omitted in equation (15), which results in underestimate of the HINLA opacity, but this effect is

small compared to the uncertainties in p. Finally, the fitting of background HI emission will underestimate the absorption temperature by $\leq$ a few K, when the HINLA happens to lie at the center of the emission. This effect could underestimate the HINLA opacity by up to 0.06 (Figure 6), but is negligible for the majority of our sources. The combined uncertainty for the derived HINLA column densities should be less than 50%.

We have developed a practical method to analyze HINLA spectra by fitting the emission and absorption portions of the spectra separately. By utilizing these two fits, the optical depth of the absorption alone can be derived without explicitly knowing the background and the foreground temperature, as long as these are equal and this material is optically thin.

4. Analysis Techniques for Spectral Lines with Small Opacities

4.1. OH Column Density

The column density of OH can be related to the optical depth of the 1667 MHz line as

$$N_{OH} = \frac{8\pi k T_x \nu^2}{A_{1667} c^3 h} \frac{16}{5} \int \tau_{1667} dV \ , \tag{16}$$

where $A_{1667} = 7.778 \times 10^{-11}$ s^{-1} is the A coefficient of this transition and T_x is its excitation temperature. The column density can be calculated from the integrated intensity (in K km s^{-1}) through

$$\frac{N_{OH}}{\mathrm{cm}^{-2}} = 2.22 \times 10^{14} \mathcal{F}_\tau \mathcal{F}_B \frac{\int T_{mb}(V) dV}{\mathrm{K\ km\ s^{-1}}} \ , \tag{17}$$

where the optical depth correction factor

$$\mathcal{F}_\tau = \frac{\int \tau dV}{\int (1 - e^{-\tau}) dV} \tag{18}$$

accounts for possible non–negligible opacity and the background correction factor

$$\mathcal{F}_B = \frac{T_x}{T_x - T_B} \tag{19}$$

is significant when the excitation temperature is not much larger than the background temperature. Often, both factors are assumed to be unity, in order to obtain an optically thin no background approximation with which to obtain the OH column density (**?**, e.g.)]knapp73, turner71

The satellite component of this Λ doubling line at 1665 MHz can be useful in determining the the optical depth and excitation temperature. For emission without anomalies, the antenna temperatures of the two components satisfy

$$\frac{T_A^{1667}}{T_A^{1665}} = \frac{1 - e^{\tau^{1667}}}{1 - e^{\tau_{1665}}} = \frac{1 - \mathcal{X}}{1 - \mathcal{X}^{0.552}} \ , \tag{20}$$

where $\mathcal{X} = e^{\tau_{1667}}$. Equation (20) gives a unique solution for $\mathcal{X}$ (Figure 6), which leads to

$$T_x = \frac{T_A^{1667}}{1 - \mathcal{X}} + T_B \ . \tag{21}$$

The ratios for our sources range from 1.2 to 1.9, with the majority being around 1.8. This confirms that we are seeing thermal emission from dark clouds and that the opacity is only modest. The background correction factor, on the other hand, is shown to be significantly larger than unity. Except for one source, the excitation temperature of OH ranges from 5 K to 9 K, giving $\mathcal{F}_B$ to be in the range 1.6 to 2.3.

Because of weaker line emission at 1665 MHz and the exponential dependence of the antenna temperatures on the optical depth, the satellite line ratio method is very sensitive to uncertainties in the spectra of the satellite component. In some cases, the line widths of the main and the satellite line are not the same, which could be explained by the low signal to noise ratio in the satellite component. To present a more self–consistent correlation study of HI and OH, we determine the OH column density (Table 3) by assuming $\mathcal{F}_\tau = 1$ and $\mathcal{F}_B = 1$. These results likely underestimate the OH column density by a factor $\simeq 2$.

4.2. $C^{18}O$ Column Density

In order to determine the molecular content of dark clouds, we have chosen an optically thin tracer, the J=1–0 transition of $C^{18}O$, for its well known abundance relative to H_2, $\sim 1.7 \times 10^{-7}$ (Frerking, Langer & Wilson 1982). The $C^{18}O$ column density in the J=1 level can be calculated from

$$\frac{N^1(C^{18}O)}{\mathrm{cm}^{-2}} = 3.72 \times 10^{14} [1 - \frac{e^{\frac{h\nu}{kT_x}} - 1}{e^{\frac{h\nu}{kT_B}} - 1}]^{-1} \frac{\int T_{mb}(V) dV}{\mathrm{K\ km\ s^{-1}}} \ , \tag{22}$$

where T_x is the excitation temperature of the J=1–0 transition, T_B is the background temperature, and the integrated intensity is corrected for the main beam efficiency. The LTE approximation is then used to justify substituting T_k for T_x for all transitions in converting $N^1(C^{18}O)$ to the total column density of $C^{18}O$. The smoothing of the FCRAO (45″ beam)

data to the Arecibo resolution gives a physical meaning to the [H]/[H_2] thus derived: it is the ratio between the total number of H atoms and H_2 molecules in a $3'$ beam (see Appendix for a detailed explanation).

5. HI Survey Statistics and Characteristics of HINLA

As described in Section 2, we surveyed 31 nearby dark clouds, unbiased in terms of HI absorption. In this sample, 23 have a clear narrow absorption dip at the same velocity as that of the OH emission (Figures 3 & 4). Four more clouds (L1498, L1506B L1622A & L1621-1) have hints of an absorption feature coincident in velocity with the OH emission, which correspond to a 'shoulder' on the HI profile (Figure 2). The remaining three clouds (B1, B5 & B213-7) have no indication of absorption, although they can be explained by foreground contamination. In short, the detection rate of HI narrow line absorption toward optically selected dark clouds is 74 to 90 percent.

This high detection rate is the first clear indication of a strong correlation between HINLA and dark clouds. Further analysis given below reveals more concrete evidence supporting this association.

5.1. Low Temperature of HINLA

There are two ways to estimate the temperature of the atomic hydrogen detected in absorption.

First, the line width of the absorption dip provides an upper limit to the kinetic temperature assuming only thermal broadening is present. The equivalent temperature,

$$T_{eq} = \frac{m_H \Delta V^2}{8 \ln(2) k} \tag{23}$$

is given in Column 13 of Table 2. There are 10 sources which have an absorption line width so narrow that the HI responsible must be thermalized, or be very close to thermalization, at a temperature lower than 15 K. The narrow line widths we have observed rule out the possibility that the HINLA could be produced in warm (e.g. cloud halo) gas with T $\simeq$ 100 K, even allowing for modestly subthermal excitation of the 21cm transition.

Subtle complications in obtaining line parameters from an absorption feature arise when the dip is on the slope of the background emission. In general, the fitted absorption line appears to peak closer to the center of the emission feature, and to appear narrower than it

really is. The corrections required in both cases are small compared to the line width of the narrow line HI absorption. We do not correct for the displacement of velocity peak, since the average effect is zero due to the randomness of the dark cloud velocity with respect to that of the background HI emission. The correction for line width is on the order of 0.04 km s^{-1} (Levinson & Brown 1980), which is only significant when calculating T_{eq} for a couple of unusually narrow–width sources. The uncertainty thus introduced in T_{eq} for L1523, L1521E and L1517B is between 0.5 K $\sim$ 1 K. For other sources, this correction can be neglected.

Second, the excitation temperature (or the spin temperature for the 21cm line) can be estimated by rewriting equation (14)

$$T_x = T_c + [pT_{HI} - \frac{T_{ab}}{1 - e^{-\tau}}]/(1 - \tau_f) \ . \tag{24}$$

The optical depth of the narrow line absorbing gas is on the order of unity. Substituting an infinite τ into the equation above overestimates T_x. For the optical depth of the foreground emission τ_f, a nominal value of 0.1 is used, which is probably an overestimate obtained by assuming the total optical depth of galactic HI emission (τ_h) to be close to unity. The upper limit of HINLA excitation temperature is thus

$$T_x^{upper} = T_c + [pT_{HI} - T_{ab}]/0.9 \ . \tag{25}$$

These upper limits are listed in Column 14 of Table 2. Compared to the temperature limit set by line width, this method has relatively large uncertainties resulting from assumptions about p and the optical depth. Nonetheless, it provides an independent estimate based on the depth of the HINLA profile. It also confirms our understanding that the majority of HINLA features come from cold gas ($\lesssim$ 40 K) with some sources in the range of 10 K.

These two estimates of temperature upper limits reveal HINLA to be associated with cold gas. A significant fraction of the sources have to has atomic gas as cold as 8–15 K. The well shielded regions of molecular cloud cores are the most likely, if not the only, sites that can plausibly contain material this cold.

5.2. HI and OH Correlation

For sources with well defined absorption features, the similarities between the OH and HINLA profiles are obvious. The two profiles are coincident in velocity with average central velocity difference equal to 0.07 km s^{-1} half of our velocity resolution.

The line widths of different species are important indicators of the conditions in the regions they are found, as well as of the extent of the regions responsible for the spectral

line in question. The well known empirical velocity–line width relations all suggest larger line widths at larger spatial scales (e.g. Larson 1981; Caselli & Myers 1995). To compare the line widths of species with very different molecular/atomic weight, it is appropriate to separate the thermal from the nonthermal contributions to the line widths. This can be done by defining the nonthermal line width as

$$\Delta V_{nt} = \sqrt{\Delta V^2 - \frac{8\ln(2)kT_k}{\mu m_H}} \ , \tag{26}$$

where ΔV is the observed FWHM of the line, μ is the molecular or atomic weight, m_H is the hydrogen mass and k is Boltzmann's constant. For HINLA, the width is that of the Gaussian fitted to the absorption profile, while for the other species we fit the emission spectra. The correction for the thermal broadening is significant for the HI due to its low mass. The nonthermal line width gives a better indicator of the spatial extent of its progenitor, since the mass dependence of the thermal broadening has been corrected for. The line width data can be found in Table 2.

It is evident that the HINLA, OH, and $C^{18}O$ line widths are well correlated, while the CI exhibits quite different behavior. The average nonthermal line width of the HINLA and of the OH are 0.85 km $s^{-1}$and 0.83 km s^{-1}, respectively. They are essentially the same as the average line width of ^{13}CO at 0.82 km s^{-1}. These results indicate that the HINLA is produced in regions of significant extinction where the molecular abundances are appreciable.

We have obtained direct information on the spatial correlation of HINLA and OH emission by extensive mapping only for one cloud, L1544, discussed below in Section 5.4. Limited evidence for spatial correlation of OH and HINLA can also be found by looking at the OFF source spectra (Figure 5). When the telescope beam is moved away from the center of each source, it is evident that the HINLA absorption dip starts to disappear along with the OH emission. There is no hint of any increase in the strength of the absorption features at the cloud boundaries, as would be expected if the gas producing the HINLA were in some peripheral zone of the clouds we have studied [4].

[4]We hesitate to use the term 'limb brightening' to describe an increase in the depth of the absorption line, but if the HI in question were in an outer 'onion skin' of the cloud, a map of the integrated area of the absorption would presumably exhibit this behavior.

5.3. Correlation with CO Isotopologues and CI

As listed in Table 2, all observed species, HINLA, OH, $C^{18}O$, and CI, have essentially the same V_{lsr} in a given cloud. The V_{lsr} of the HINLA and of the $C^{18}O$ are plotted in Figure 7. The root mean square separation of our data points from the line of equal velocities is 0.03 km s^{-1}, which is small compared to both the line width and the velocity resolution.

As traced by the line widths, the spatial distributions within the clouds of the CO isopologues, the HINLA, and the HI appear to be somewhat different. As mentioned above, HI, OH, and ^{13}CO have, on average, the same line width. $C^{18}O$ has the narrowest line width ($< \Delta V > \sim 0.64$ km s^{-1}), presumably tracing the innermost core. The CO line is wider with $< \Delta V > = 1.2$ km s^{-1}, while the CI line is much wider still with $< \Delta V > = 2.3$ km s^{-1}. The large nonthermal line width of the CI confirms this species to be a tracer of PDR regions, where more prominent turbulence exists. HINLA seems to be mixed with relatively quiescent molecular material at higher extinction.

For individual sources, a positive correlation exists between the line width of OH and of HINLA, as shown in the upper left panel of Figure 8. The probability of the null hypothesis (the two being uncorrelated) is $r = 3.6\times10^{-5}$; the linear correlation coefficient is 0.76. A similar correlation exists between the OH line width and that of $C^{18}O$. In contrast, no such correlation exist between the OH and CI line widths. Again assuming a linear correlation, the null hypothesis is very likely ($r = 0.49$).

For the column densities, only OH and $C^{18}O$ are definitely positively correlated. For HINLA, there is a suggestion of a positive correlation, but the scatter is large due to the uncertainty in the background line profile and to the foreground contamination (Section 3). For CI, the assumption of small optical depth has not been tested in our study and thus may cause large uncertainties. The current data set does not definitively answer all questions about the correlation between column densities of the different species, a subject which deserves additional consideration.

5.4. L1544

To get a better idea of the spatial correlation of HINLA and molecular tracers, we mapped the quiescent dark cloud L1544. This object has relatively narrow line widths in molecular tracers (ΔV(CO) = 1.0 km s^{-1}; $\Delta V(C^{18}O)$ = 0.44 km s^{-1}). It is usually characterized as starless, due to there being no clear association with an IR source (Ward-Thompson, Scott, Hills, & André 1994). The inner 5′ core region around the center of L1544 has been well studied and found to exhibit molecular depletion and infall motions (Caselli,

Walmsley, Zucconi, et al. 2002; Tafalla et al. 1998).

We mapped an extended region of L1544, which is the same area as outlined by extinction (Snell 1981). The RMS of our HI and OH spectra are smaller than 0.1 K. At the cloud periphery, the OH 1667 MHz emission is generally weaker than 3 σ. All three tracers, OH, HINLA, and $C^{18}O$ delineate the same cloud (Figure **??**). The H_2 column density in the center of this cloud derived from $C^{18}O$ and assumed standard fractional abundance is 6.5×10^{21} cm^{-2}. Taking dimensions of the cloud core of 9′ by 16′ gives a characteristic size of 0.49 pc at an assumed distance of 140 pc. This results in a characteristic volume density $n(H_2) = 4.3\times10^3$ cm^{-3}.

For a spherical cloud of uniform density in virial equilibrium ignoring magnetic fields and external pressure, the H_2 density is given by

$$\frac{n_v(H_2)}{\mathrm{cm}^{-3}} = 2.03 \times 10^3 \frac{1}{\mu} [\frac{\Delta V/(\mathrm{km\ s}^{-1})}{R/(\mathrm{pc})}]^2 \ , \tag{27}$$

where ΔV is the FWHM line width, R is the cloud radius, and μ is the mean molecular weight. Substituting the appropriate values yields $n_v(H_2) = 2.9 \times 10^3$ cm^{-3}. This is in reasonable agreement with the average density derived above, and suggests that this cloud is in, or not far, from virial equilibrium.

The secondary maximum in OH located around offsets (-8′, 3′) is due to a localized increase in the line width, indicating an increase in turbulence. At the center of the cloud, the line width of the 1667 MHz OH emission is 0.47 km s^{-1}, while at (-8′, 3′), it is 0.70 km s^{-1}. This second, more turbulent peak in the OH column density does not correspond to an enhancement in either $C^{18}O$ or HINLA. A likely scenario is that the OH traces a low extinction envelope, which exhibits fluctuations in MHD or some other kind of turbulence, while $C^{18}O$ represent the total column density of quiescent material. HINLA produced by cosmic ray dissociation (see Section 6 below), which is unaffected by extinction, should also be able to trace the highest column density regions. On the other hand, if HINLA is produced mainly by photodissociation in the envelope, a limb brightening effect should appear. Such an effect is not seen. Our composite image of L1544 is consistent with material responsible for the HINLA being mixed with the quiescent gas.

6. Atomic Hydrogen Density in Molecular Clouds

The majority of molecular hydrogen in the ISM is thought to be formed by reactions on dust grains. This process is also the major destruction pathway for hydrogen atoms. The

steady state H_2 production rate (cm^{-3} s^{-1}) R_{H_2} can be written as

$$R_{H_2} = 0.5 n_g n_1 \sigma v S \eta \ , \tag{28}$$

where n_g is the grain number density, n_1 is the HI density in the gas phase, σ is the grain cross section, v is the relative velocity between H atom and grains (essentially the velocity of H), S is the sticking probability of an H atom on a grain, and η is the formation efficiency. The total density of hydrogen atoms is $n_H = (n_1 + 2n_2)$, where n_2 is the density of hydrogen molecules. The grain and proton number densities are related through $n_g = g n_H$. The value of g depends on the grain model and gas conditions. A 'standard' dust grain is taken to have a radius of 0.1 μm and a density of 3 g cm^{-3}. In a molecular cloud, we can reasonably assume the following gas conditions: [He]/[H] equal to 0.09, most hydrogen gas in the form of H_2, and an gas to dust mass ratio of 100. Based on these assumptions about the dust grains and the gas, we determine g to be 1.8×10^{-12}.

In the standard picture of H_2 formation (Hollenbach & Salpeter 1970), the time scale for H atoms deposited on the grain to 'cover' the grain surface through tunneling processes is much shorter than the residence time of an adsorbed H atom. Since the H_2 formation reaction is exothermic (4.5 ev released), η is taken to be 1 in their model as long as there are more than two H atoms on a grain. Equation 28 with a near unity η works well in diffuse clouds with S$\sim$0.3 (Hollenbach & Salpeter 1971). A recent study of sticking probability on icy surfaces gives S close to unity at low temperatures (Buch & Zhang 1991). We therefore use $S = 0.5$ in the following discussion. Therefore, the equation

$$R_{H_2} = 2.06 \times 10^{-18} n_H n_1 \sqrt{T} \ , \tag{29}$$

where T is the gas temperature, has been used as the canonical basis for explaining the fast formation of H_2 and in constructing chemical networks.

For typical dark cloud conditions with temperature of 10 K, $n_H \sim 10^4$ cm^{-3}, the HI to H_2 conversion time scale, n_1/R_{H_2}, is approximately 0.5 million years. Such a rapid conversion leaves an essentially 'molecular' cloud in which the atomic component is maintained by cosmic rays in a steady state. The destruction rate of H_2 is ξn_2 (cm^{-3} s^{-1}), where $\xi = 3 \times 10^{-17}$ s^{-1} is the cosmic ray ionization rate. This parameter has approximately a factor of 3 uncertainty associated with it, as indicated by the varied results and range of fits obtained for different sources and models by e.g. Caselli, Walmsley, Terzieva, & Herbst (1998), Caselli, Walmsley, Zucconi, et al. (2002). In a steady state and assuming $n_2 \gg n_1$,

$$\dot{n_2} = 2.06 \times 10^{-18} \times 2 n_2 n_1 T^{1/2} - \xi n_2 = 0 \ , \tag{30}$$

which, for 10 K, gives n_1 to be 2.3 cm^{-3}.

This HI density is *independent* of the environmental density [5]. Therefore the entire region containing molecular material can contain cold HI and be capable of producing HINLA, with essentially an equal contribution per cm of path along the line of sight. In our sample of clouds, the average column density of HINLA is 7.2×10^{18} cm^{-2}. We adopt an angular size for the region with absorbing HI of $15'$, which is consistent with the typical size of Lynds clouds and Bok globules in the Taurus complex. This corresponds to a physical dimension equal to 0.6 pc at a distance of 140 pc. The average H_2 gas density which we derive from the average column density of $C^{18}O$ and fractional abundance 1.7×10^{-7} is equal to 2.5×10^3 cm^{-3}. The average HI fractional abundance [HI]/[H_2] in the dense molecular gas predicted from the standard theory is 9.2×10^{-4}. This is in reasonable agreement with the observed result 1.5×10^{-3} (see Table 3 and Figure **??**).

Another obvious process for producing atomic hydrogen associated with molecular clouds is photodissociation. In a plane parallel PDR model with microturbulence (Wolfire, Hollenbach, & Tielens 1993; Jackson et al. 2002), a large fractional abundance of HI ($> 10^{-2}$) can be produced at low extinctions ($A_v < 2$). We do not see this HI envelope, either in total column density or in morphology. One possible explanation is that the conditions in such regions are much less favorable for production of HINLA than the cold, quiescent regions of the clouds. If we ignore foreground and background absorption as well as any continuum, we see from equations (10) and (13) that the magnitude of the absorption line from optically thin, thermalized gas responsible for the HINLA in the cloud is

$$\frac{T_{ab}^0}{\mathrm{K}} = 5.3\times10^{-19}\frac{N(\mathrm{HI})/(\mathrm{cm}^{-2})}{\Delta V/(\mathrm{km\ s}^{-1})}[\frac{T_{HI}-T_x}{T_x}]\ , \tag{31}$$

where T_x is the excitation temperature of the atomic hydrogen. As the temperature in the PDR region rises, so does T_x, and the absorption intensity drops; as T_x approaches the background temperature, the drop becomes precipitous. In these externally ionized and heated regions, it is reasonable that the turbulence, and hence the line width, is considerably greater than in the quiescent cloud material, which also weakens the absorption per hydrogen atom.

As pointed out by Wolfire, Hollenbach, & Tielens (1993), the microturbulent model has difficulty in reproducing CO 1–0 line profiles. Another scenario is clumpy cloud models with macroturbulence. The difficulty with such models is that the observed line profiles are usually very smooth, which is hard to reproduce by a clumpy structure. It would be very

[5]This is by no means a new result; e.g. Solomon & Werner (1971) showed that a constant n_1 was to be expected, although their value was more than an order of magnitude larger due to the large value of the cosmic ray ionization rate which they adopted.

interesting to see the predictions of PDR models and radiative transfer calculations with numerous tiny clumps.

7. Discussion

Through observations of HINLA, we have identified cold atomic hydrogen associated with molecular clouds. A detailed explanation of HINLA and related molecular species would require comprehensive models, which may involve PDR, clumpy structure, gas and grain surface chemistry (Ruffle & Herbst 2000), and possibly other effects such as turbulent diffusion (Willacy, Langer & Allen 2002). Accurate determination of the abundance of cold HI and its spatial distribution would constitute a difficult test of the chemistry and physics of 'molecular' clouds.

A steady state calculation using standard cosmic ray rate and H_2 formation rate is shown to produce approximately the amount of cold HI observed. The data do suggest, however, that there may be a need for modest additional sources of atomic hydrogen in cold molecular regions.

The simple steady state model may not be an accurate or complete picture, however. Our own chemical simulation including grain surface reactions (Li & Goldsmith 2002). and laboratory experiments (Pirronello et al. 1999), suggest slower H_2 formation, which will produce a higher HI density in moderately–aged and dense cores. Thus, it is possible that the HI fractional abundance we have observed can be used to put an upper age limit on the clouds. The question of whether the H_2 formation rate does slow down in dense cores can be answered by observations at higher spatial resolution ($< 1'$), which will either identify HINLA features correlated with high density tracers, or show HINLA to be smooth on such scales.

HINLA traces different population of neutral hydrogen from that constituting the warm HI halos also associated with molecular clouds (Andersson, Wannier, & Morris 1991). The HI halos are mostly seen by virtue of the enhancement of HI emission around molecular clouds. Statistically, the HI emission maxima have been shown to lie outside the clouds as defined by their CO emission (Wannier, Lichten, Andersson, & Morris 1991). Such halos have to be warm to be seen in HI emission with the galactic background. In fact, the absorption measurements against continuum sources place the halo temperature around B5 to be 70 K (Andersson, Roger & Wannier 1992), well above the temperatures of HINLA. HI halos are also shown to be much more much more spatially extended than is the CO emission (Andersson, Wannier, & Morris 1991). This is also in contrast with our observations

of HINLA, which place cold HI inside CO clouds, a region region of size between those characteristic of $C^{18}O$ and ^{13}CO emission.

HINLA could be a very good tracer with which to measure the magnetic field in dark clouds. The most successful Zeeman tracer for dark clouds is OH emission at 1667 and 1665 MHz. HINLA is about 10 times stronger than OH emission with a comparably large Landé g factor (Kazès & Crutcher 1986). Its line widths are similar, as is its spatial extent, indicating that it should be sensitive to the magnetic field in largely the same regions producing the OH emission. We should thus expect Zeeman studies of HINLA to allow extensive, sensitive observations of the magnetic field in molecular clouds.

8. Conclusions

We have surveyed 31 dark clouds using Arecibo, FCRAO, and SWAS. The analysis of these data show the following.

1. The 21cm HI narrow line absorption having line width smaller than 2 km s^{-1} is a widespread phenomenon, detected in over 80% of our sample of dark clouds in the Taurus/Perseus region. We use the term HINLA to distinguish the narrow line absorption from broader absorption features seen in other surveys of HI throughout the Galaxy.

2. The atomic hydrogen producing the narrow line absorption has significant column density with $N(\mathrm{HINLA}) \sim 7 \times 10^{18}$ cm^{-2}.

3. The gas responsible for the HINLA is at low temperatures, between 10 and 25 K. Some sources (L1521E, L1512, L1523) must be thermalized at temperatures close to or lower than 10 K.

4. The nonthermal line width of HINLA is comparable to the line width of ^{13}CO, only slightly larger than that of $C^{18}O$, and is smaller than the line widths of CO or CI. This suggests that HINLA is produced by cold atomic hydrogen in regions of moderate extinctions with A_v larger than a few.

5. In the one cloud for which we have detailed mapping data, L1544, HINLA is morphologically similar to $C^{18}O$.

6. The low temperature, the absence of increased absorption at cloud edges, and the narrow line width of HINLA suggest that the atomic hydrogen producing HINLA is mixed with the gas in cold, well–shielded regions of molecular clouds.

7. Zeeman measurements of HI narrow line absorption should be useful probes of the magnetic field in molecular clouds.

A. Telescope Efficiencies and Derived Column Densities

A.1. Antenna Temperature and Antenna Theorem

The power, P (erg s^{-1}) , received by an antenna [6] from a source having brightness (erg cm^{-2} s^{-1} sr^{-1} Hz^{-1}) distribution $B(\Omega)$ is

$$P = \frac{1}{2} A_e \Delta\nu \iint B(\Omega) P_n(\Omega) d\Omega \ , \tag{A1}$$

where P_n is the normalized antenna power pattern and we assume the atmosphere to be transparent. All quantities are assumed to be frequency independent over the relatively narrow range of frequencies, $\Delta\nu$. The above equation can be viewed as the definition of the antenna effective area, A_e. The antenna temperature scale is defined through

$$P = kT_A \Delta\nu \ , \tag{A2}$$

which gives us

$$T_A = \frac{A_e}{2k} \iint B(\Omega) P_n(\Omega) d\Omega \ . \tag{A3}$$

For a source having temperature T_s in direction Ω,

$$B(T_s) = \frac{2h\nu^3/c^2}{e^{h\nu/kT_s(\Omega)} - 1} \ . \tag{A4}$$

In the Rayleigh–Jeans limit, $h\nu/kT_s << 1$, and the antenna temperature becomes

$$T_A = \frac{A_e}{\lambda^2} \iint T_s(\Omega) P_n(\Omega) d\Omega \ , \tag{A5}$$

For a uniform source which fills the entire antenna pattern

$$T_A = \frac{A_e \Omega_A}{\lambda^2} \frac{h\nu/k}{e^{h\nu/kT_s} - 1} \ , \tag{A6}$$

where Ω_A is the antenna solid angle, defined by the integral of $P_n(\Omega)$ over all solid angle. In the Rayleigh-Jeans limit, this reduces to

$$T_A = \frac{A_e \Omega_A}{\lambda^2} T_s \ . \tag{A7}$$

[6] more precisely, from a single polarization receiver coupled to a single spatial mode collected by the antenna

The antenna effective area and the solid angle subtended by the beam it produces are related through the antenna theorem (Kraus 1966; Goldsmith 2003)

$$A_e \Omega_A = \lambda^2 \epsilon_r \ , \tag{A8}$$

where ϵ_r is the ohmic loss efficiency ($1 - \epsilon_r$ = fraction of power lost by absorption). For an ideal antenna, the ohmic loss is zero and $\epsilon_r = 1$, which simplifies the antenna theorem to its canonical form. In practice, there are always losses and it could be confusing to omit ϵ_r from the antenna theorem, because A_e is measured through Eq. (A10), in which the ohmic loss is included.

For a lossless antenna, the antenna theorem simplifies equation A7 to

$$T_A = T_s \ ; \tag{A9}$$

this is the basis for antenna calibration by means of thermal loads that fill the beam (usually achieved by using loads which cover the feed horn).

For a source of arbitrary size, relating the measured T_A to the source temperature T_s, requires that the effective area A_e be measured. For radio telescopes, this is accomplished by observing a point source (source solid angle much less than that of the antenna beam) of known flux density S (erg s^{-1} cm^{-2} Hz^{-1}), and determining

$$A_e = \frac{2kT_A}{S} \ . \tag{A10}$$

A.2. Antenna Efficiencies and Column Density Determination

The structure of an antenna power pattern can be measured by scanning a strong source. Although helpful in understanding the measured signal, the beam map alone is not sufficient in converting antenna temperatures to source temperatures. The other element in the convolution, the source structure, is almost always not known a priori. Without information about the source structure on scales comparable to or smaller than the beam, several efficiencies can be defined to characterize the antenna response, for reasonable limits of the source structure.

From a point source of known flux density S, the effective area A_e of the antenna can be measured as in equation (A10). This gives the power response of the antenna to a point source. Usually, it is presented as the antenna efficiency $\epsilon_A = A_e/A_p$, relating the effective area to the physical area, A_p. For the Arecibo antenna at L-band, we obtain $A_e = 2.54{\times}10^4$ m^2 through observations of a set of calibration quasars. The appropriate physical area is, in

this case, the elliptical area 213 m x 237 m in size illuminated by the Gregorian feed system; $A_p = 3.97{\times}10^4$ m^2. This yields an aperture efficiency $\epsilon_A = 0.64$.

The antenna response to an extended source (solid angle Ω_s) can be described in terms of a coupling efficiency

$$\epsilon(\Omega_s) = \frac{\iint\limits_{\Omega_s} P_n(\Omega) d\Omega}{\iint\limits_{4\pi} P_n(\Omega) d\Omega} \ . \tag{A11}$$

For a uniform source,

$$T_s^0 = \frac{T_A}{\epsilon(\Omega_s)} \ . \tag{A12}$$

When the source solid angle Ω_s includes precisely the main beam, the coupling efficiency is the main beam coupling efficiency, generally referred to as the beam efficiency, given by

$$\epsilon_{mb} = \frac{\Omega_{mb}}{\Omega_A} = \frac{\Omega_{mb}\epsilon_A A_p}{\lambda^2} \ . \tag{A13}$$

The antenna temperature thus corrected is called main beam temperature T_{mb}. From beam maps and ϵ_A, we derive the main beam efficiency of the Arecibo antenna to be 0.6 at L–band.

The application of efficiencies depends on not only on the source size, but also on the scientific objective. A specific common and useful situation is to infer the column density from an optically thin tracer. In this case, $T_s = T_x\tau$, relates the source brightness temperature to the excitation temperature and the optical depth. For small τ, T_s is proportional to τ and hence to the column density.

For this study (as in many others) we want to know the characteristic column density of gas in the cloud being observed. A reasonable starting point for assessing the uncertainties resulting from a poorly–known source size is to assume a uniform circular source, together with an azimuthally symmetric radiation pattern for the antenna. Since the source is uniform, the antenna temperature is related to the source brightness temperature via the coupling efficiency, $T_A = T_s\epsilon(\theta_s)$, where θ_s is the angular radius of the source. If we consider a source of a given column density, N, the antenna temperature that it will produce is

$$T_A = \epsilon(\theta_s) G N \ , \tag{A14}$$

where G is the constant that converts column density to brightness temperature.

Since we know that the optical depth is proportional to the column density, if we assume an angular radius for the source equal to θ_a, the column density that we would derive is given

by

$$N_a = \frac{T_A}{\epsilon(\theta_a)G} \ . \tag{A15}$$

We can relate the column density derived using the assumed source size to the true column density by combining these equations:

$$\frac{N_a}{N} = \frac{\epsilon(\theta_s)}{\epsilon(\theta_a)} \ . \tag{A16}$$

It is common practice to make the assumption that the source just fills the main beam. This is certainly reasonably well justified in the present study where our limited mapping data confirms that the sources are extended, and that the distribution is relatively smoothly tapered. In this case, the ratio of the true column density to that derived from assuming the uniform source fills the main lobe of the antenna beam is

$$\frac{N_{mb}}{N} = \frac{\epsilon(\theta_s)}{\epsilon(\theta_{mb})} = \frac{\epsilon(\theta_s)}{\epsilon_{mb}} \ . \tag{A17}$$

For sources larger than the solid angle subtended by the main beam, $\epsilon(\theta_s)$ will be larger than ϵ_{mb}, and hence N_{mb} will be greater than N. There are at least two contributions of the power pattern outside the main lobe: the diffraction sidelobes and the so–called error beam resulting from surface imperfections. A third source, spillover past the subreflector edge in a Cassegrain system, is not relevant for the configuration of the Arecibo Gregorian. Usually the size of the error beam is on the order of degrees, much larger than the source size, which makes the error–beam contribution to the total power negligible. This is true for the HINLA sources of interest here, although it may not strictly be true for the Galactic 21cm emission itself, which is extremely extended. The main beam efficiency $\simeq 0.6$ for the Arecibo Gregorian system at L–band. Maps made of the antenna pattern indicate that the coupling efficiency even for sources many times the size of the main lobe is only $\simeq 0.75$. In summary, by applying the main beam efficiency, we would overestimate the column density of a very extended source (assumed uniform and circular) by no more than $\simeq 25$ percent.

For small sources with $\theta_s \ll \theta_{mb}$, $\epsilon(\theta_s)$ can, in principle, be much smaller than ϵ_{mb}. In this limit of pointlike sources, N_{mb} will be a severe underestimate of the source column density. Again, there is no suggestion of unresolved sources in this sample, but the issue of small–scale structure does remain. This can be resolved only with higher angular resolution observations, but our estimation here is that using the main beam efficiency will underestimate the column density by at most a modest factor. In conclusion, using ϵ_{mb} to correct the observed antenna temperature appears to be a nearly optimum procedure given what we know about these sources at the present time.

REFERENCES

Allison, A.C. & Dalgarno, A. 1969, ApJ, 158, 423

Andersson, B.-G., Roger, R. S. & Wannier, P. G. 1992, A&A, 260, 355

Andersson, B.-G., Wannier, P. G., & Morris, M. 1991, ApJ, 366, 464

Barnard, E. E. 1927, Chicago: University of Chicago Press, *Catalogue of 349 Dark Objects in the Sky*

Buch, V. & Zhang, Q. 1991, ApJ, 379, 647

Burton, W. B. 1988, in Galactic and Extragalactic Radio Astronomy, ed. Kellermann, K. I. & Verschuur, G. L.

Caselli, P., Hasegawa, T. I. & Herbst, E. 1998, ApJ, 495, 309

Caselli, P. & Myers, P. C. 1995, ApJ, 446, 665

Caselli, P., Walmsley, C.M., Terzieva, R., & Herbst, E. 1998, ApJ, 499, 234

Caselli, P., Walmsley, C.M., Zucconi, A., Tafalla, M., Dore, L., & Myers, P.C. 2002, ApJ, 565, 344

Chièze, J.-P. & Pineau des Forêts, G. 1989, A&A, 221, 89

Chromey, F. R., Elmegreen, B. -G. & Elmegreen, D. M. 1989, AJ, 98, 2203

Field, G.B. 1958, Proc. IRE, 46, 240

Goldsmith, P. F. 2003 in NAIC–NRAO School on Single–Dish Radio Astronomy, ed. Stanimirovic, S., Goldsmith, P.F., Altschuler, D. & Salter, C. (San Francisco CA: Astronomical Society of the Pacific), in press

Frerking, M. A., Langer, W. D. & Wilson, R. W. 1982, ApJ, 262, 590

Goodman, A. A., Crutcher, R. M., Heiles, C., Myers, P. C., & Troland, T. H. 1989, ApJ, 338, L61.

Hasegawa, T. I., Herbst, E. & Leung, C. M. 1992, ApJS, 82, 167

Herrmann, F., Madden, S.C., Nikoa, T., et al. 1997, ApJ, 481, 343

Hobbs, L. M., Morgan, W. W., Albert, C. E. & Lockman, F. J. 1982, ApJ, 263, 690

Hollenbach, D. & Salpeter, E. E. 1970, J. Chem. Phys., 53, 79

Hollenbach, D. & Salpeter, E. E. 1971, ApJ, 163, 155

Hollenbach, D. J., Werner, M. W., & Salpeter, E. E. 1971, ApJ, 163, 165

Jackson, J. M., Bania, T. M., Simon, R., Kolpak, M., Clemens, D. P., & Heyer, M. 2002, ApJ, 566, L81

Katz, N., Furman, I., Biham, O., Pirronello, V. & Vidali, G. 1999, ApJ, 522, 305

Kazès, I. & Crutcher, R. M. 1986, A&A, 164, 328

Knapp, G. R. & Kerr, F. J. 1973, AJ, 78, 453

Knapp, G. R. 1974, AJ, 79, 541

Kraemer, K. E., Jackson, J. M., & Lane, A. P. 1998, ApJ, 503, 785

Larson, R. B. 1981, MNRAS, 194, 809

Kraus, J.D. 1966, *Radio Astronomy* (New York, NY: McGraw–Hill)

Kulkarni, S. R. & Heiles, C. 1988, in Galactic and Extragalactic Radio Astronomy, ed. Kellermann, K. I. & Verschuur, G. L. (New York NY: Springer)

Lee, C. W. & Myers, P. C. 1999, ApJS, 123, 233

Levinson, F. H. & Brown, R. L. 1980, ApJ, 242, 416

Li, D. & Goldsmith, P.F. 2002, in preparation

Lis, D.C., Keene, J., Phillips, T.G., Schilke, P., Werner, M.W., & Zmuidzinas, J. 2001, ApJ, 561, 823

Liseau, R., White, G.J., Larsson, B., et al. 1999, A&A, 344, 342

Lockman, F. J. 1984, ApJ, 283, 90

Lynds, B. T. 1962, ApJS, 7, 1

McCutcheon, W. H., Shiner, W. L. H. & Booth, R. S. 1978, MNRAS, 185, 755

Minn, Y. K. 1981, A&A, 103, 269

Myers, P. C., Ho, P. T. P., Schneps, M. H., Chin, G., Pankonin, V. & Winnberg, A. 1978, ApJ, 220, 864

Pirronello, V., Liu, C., Roser, J. E. & Vidali, G. 1999, A&A, 344, 681

Plume, R. et al. 2000, ApJ, 539, L133

Purcell, E. M. & Field, G. B. 1956, ApJ, 124, 542

Pöppel, W. G. L., Rohlfs, K. & Celnik, W. 1983, A&A, 126, 152

Pratap, P., Dickens, J. E., Snell, R. L., Miralles, M. P., Bergin, E. A., Irvine, W. M., & Schloerb, F. P. 1997, ApJ, 486, 862.

Riegel, K. W. & Crutcher, R. M. 1972, A&A, 18, 55

Ruffle, D. P. & Herbst, E. 2000, MNRAS, 319, 837

Saito, T., Ohtani, H. & Tomita, Y. 1981, PASJ, 33, 327

Sherwood, W. A. & Wilson, T. L. 1981, A&A, 101, 72

Snell, R. L. 1981, ApJS, 45,

Solomon, P.M. & Werner, M.W. 1971, ApJ, 165, 41 121

Tafalla, M., Mardones, D., Myers, P. C., Caselli, P., Bachiller, R., & Benson, P. J. 1998, ApJ, 504, 900

Turner, B. E. & Heiles, C. 1971, ApJ, 170, 453

Wannier, P. G., Lichten, S. M., Andersson, B.-G., & Morris, M. 1991, ApJS, 75, 987

Wannier, P. G., Lichten, S. M., & Morris, M. 1983, ApJ, 268, 727

Ward-Thompson, D., Scott, P. F., Hills, R. E., & André, P. 1994, MNRAS, 268, 276

Wild, J. P. 1952, ApJ, 115, 206.

Willacy, K., Langer, W. D. & Allen, M. 2002, submitted to ApJ

Williams, J. P., Bergin, E. A., Caselli, P., Myers, P. C. & Plume, R. 1998, ApJ, 503, 689.

Wilson, T. L. & Minn, Y. K. 1977, A&A, 54, 933

Winnberg, A., Grasshoff, M., Goss, W. M. & Sancisi, R. 1980, A&A, 90, 176

Wolfire, M. G., Hollenbach, D., & Tielens, A. G. G. M. 1993, ApJ, 402, 195

Young, J. S., Goldsmith, P. F., Langer, W. D., Wilson, R. W., & Carlson, E. R. 1982, ApJ, 261, 513.

AAS LaTeX macros v5.0.

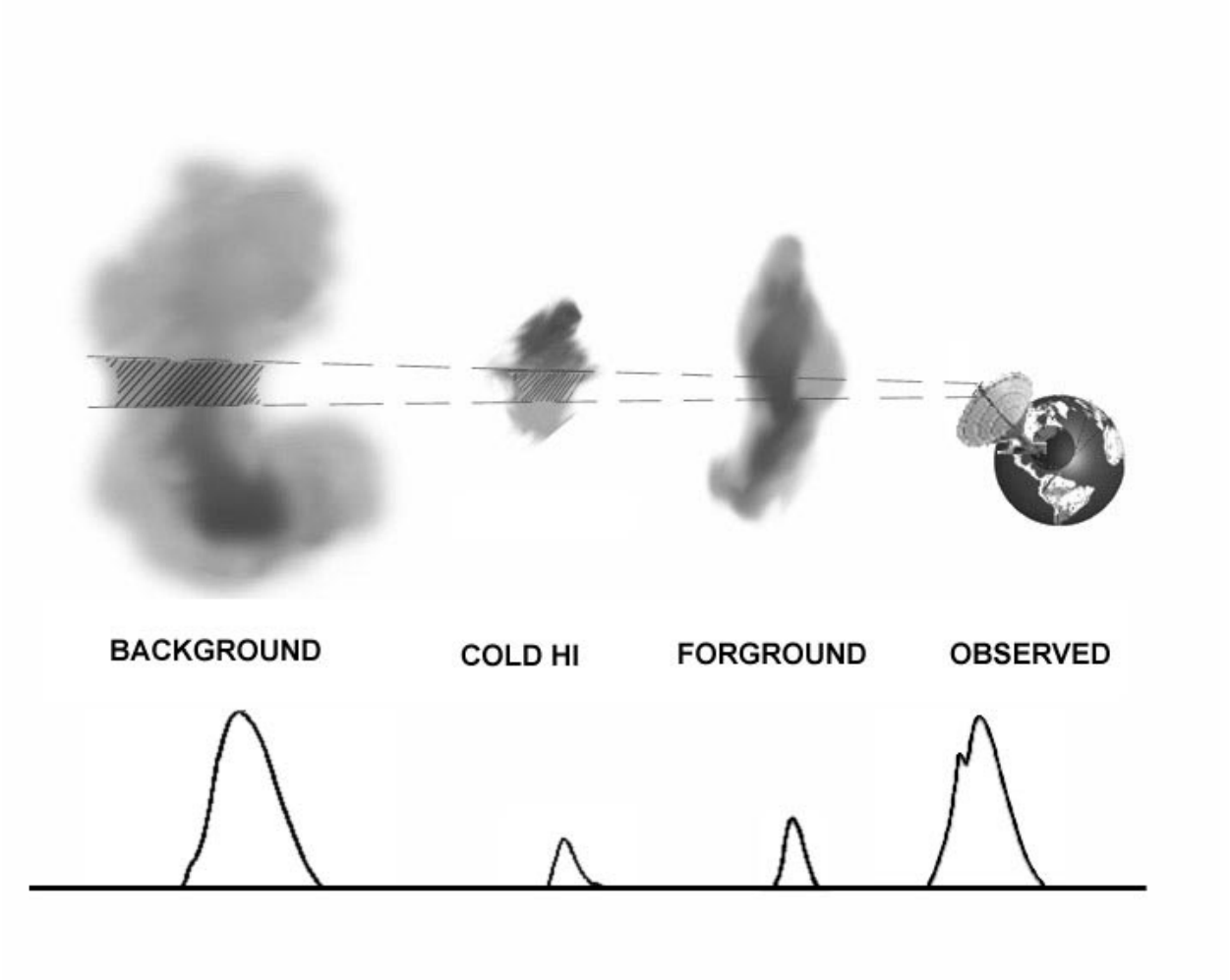

Fig. 1.— Three–body radiative transfer configuration.

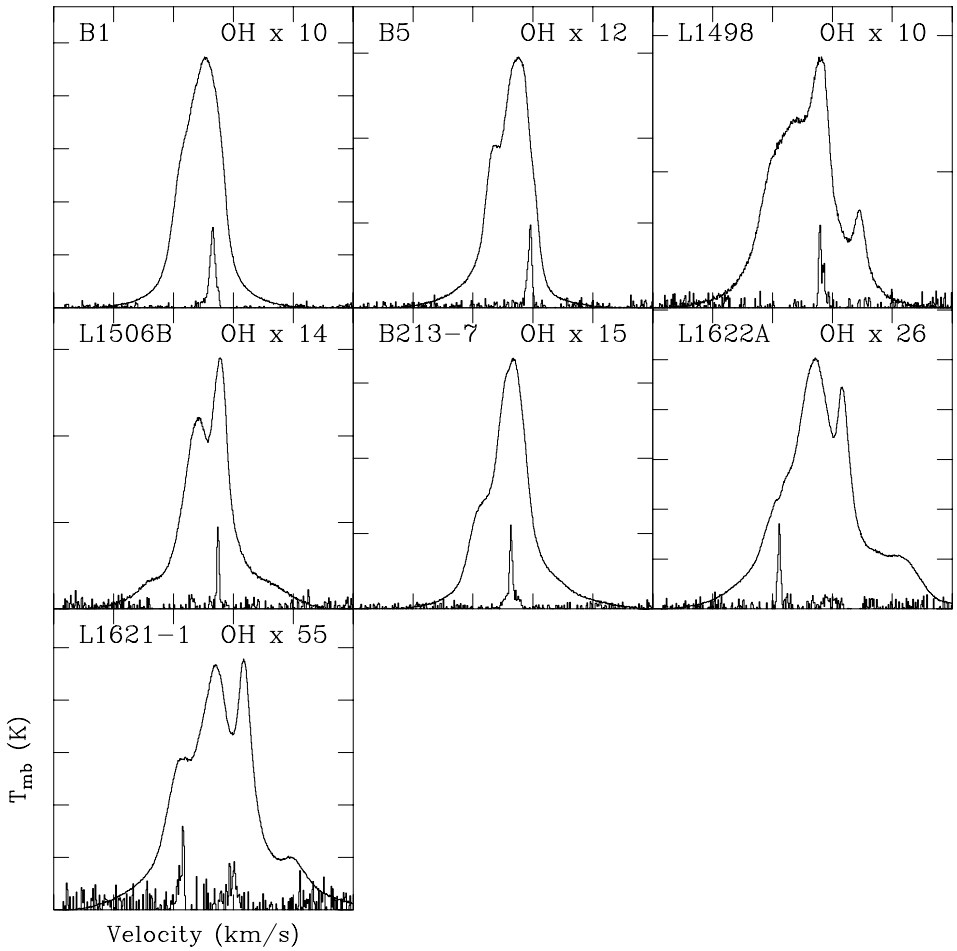

Fig. 2.— Sources without a clear narrow line HI absorption dip. The offsets from the source centers (Table 1) are indicated at the right of the source name as (ΔRA, ΔDEC) in arc minutes. The number following "OH x" is the factor by which the OH line has been multiplied in order to be visible on the plot. The X axes are centered on the V_{lsr} of the HINLA (given in Table 2) and each tick mark represents 10 km s^{-1}. The units of the Y axes are main beam antenna temperature, and each tick mark represents 10 K.

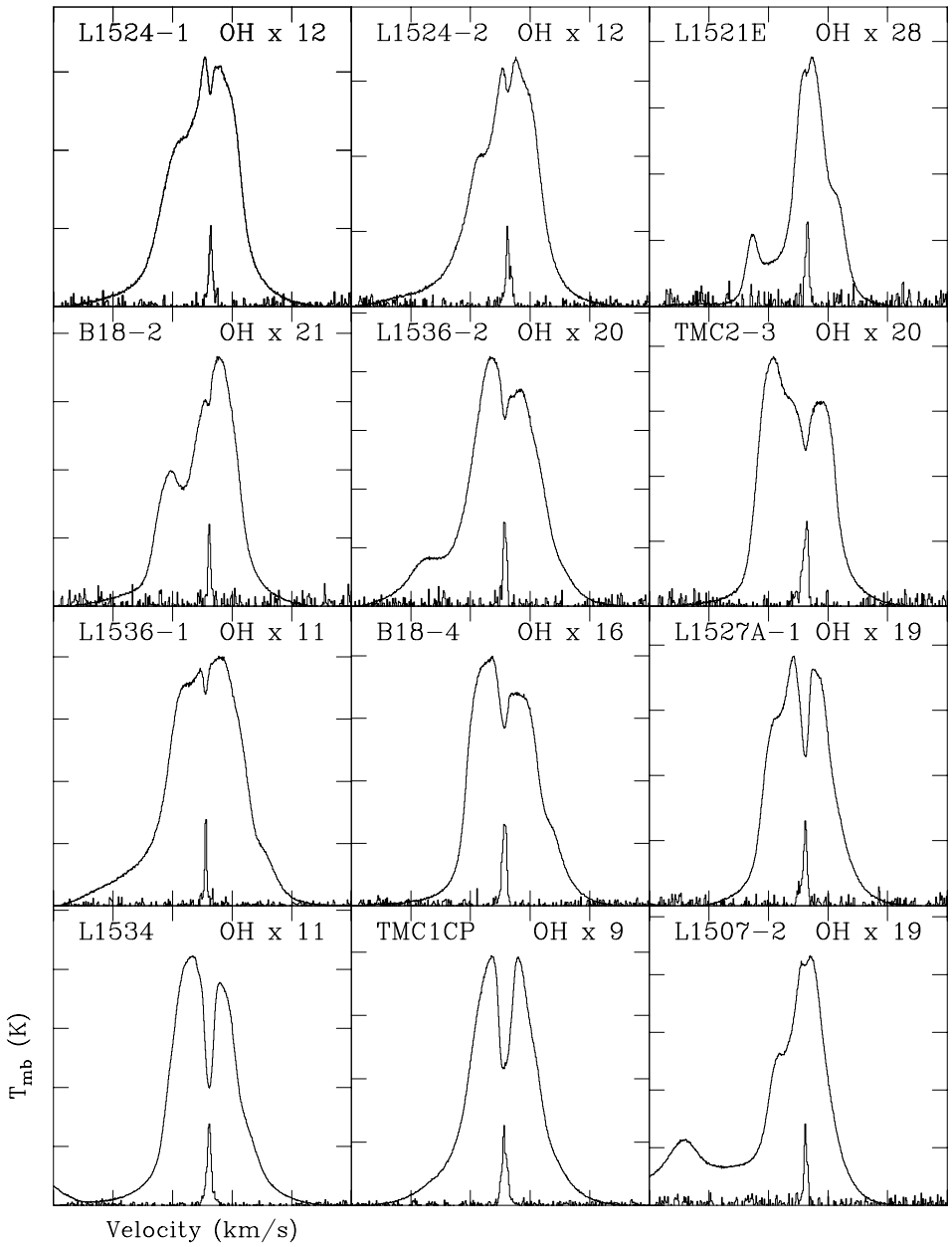

Fig. 3.— Sources with clear narrow line HI absorption. The axes are the same as in Figure 2.

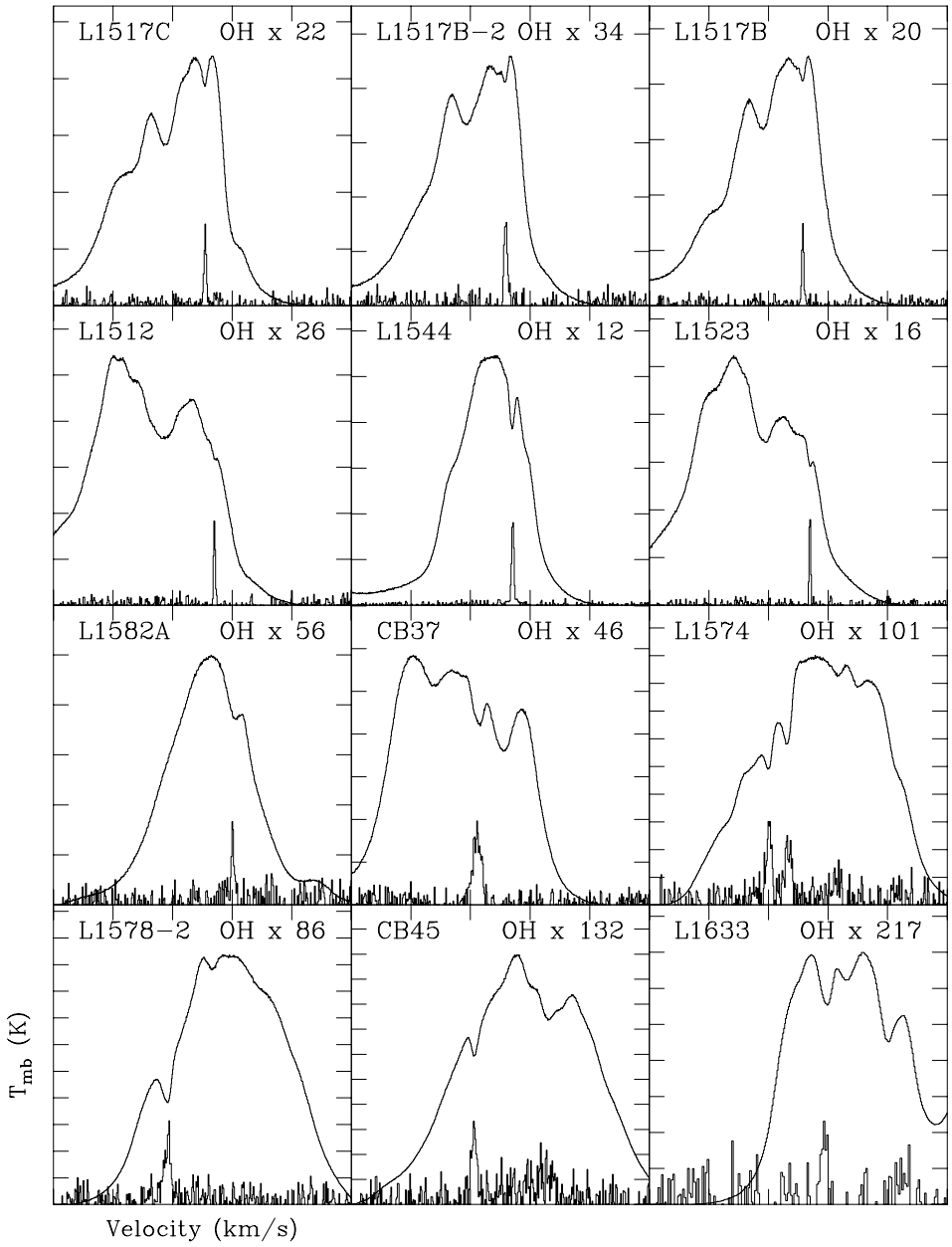

Fig. 4.— Sources with clear HINLA (continued).

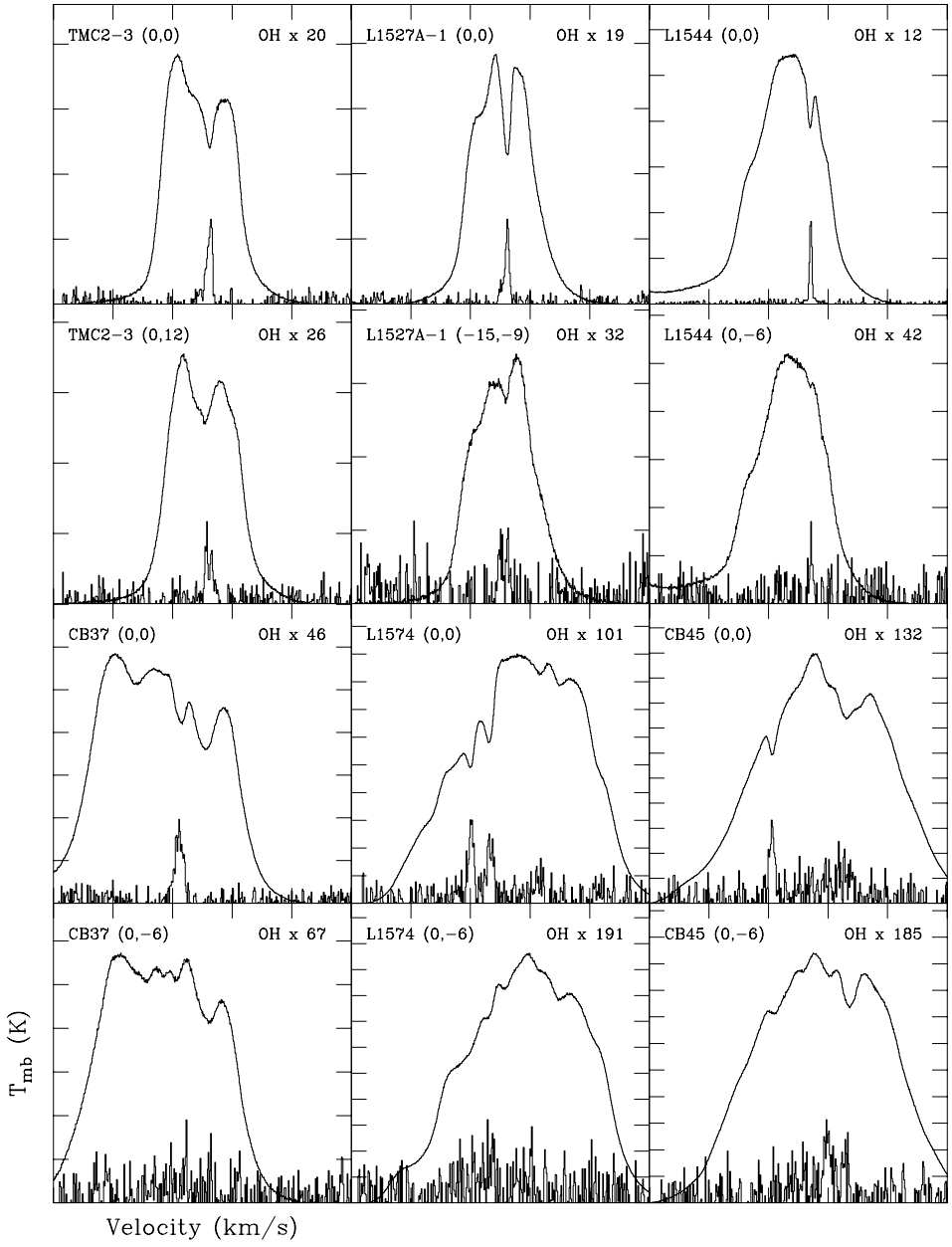

Fig. 5.— Selected sources together with associated OFF positions. The narrow HI absorption feature and OH emission line visible in the ON source spectra are almost entirely absent in the OFF source spectra. The axes are the same as in Figure 2.

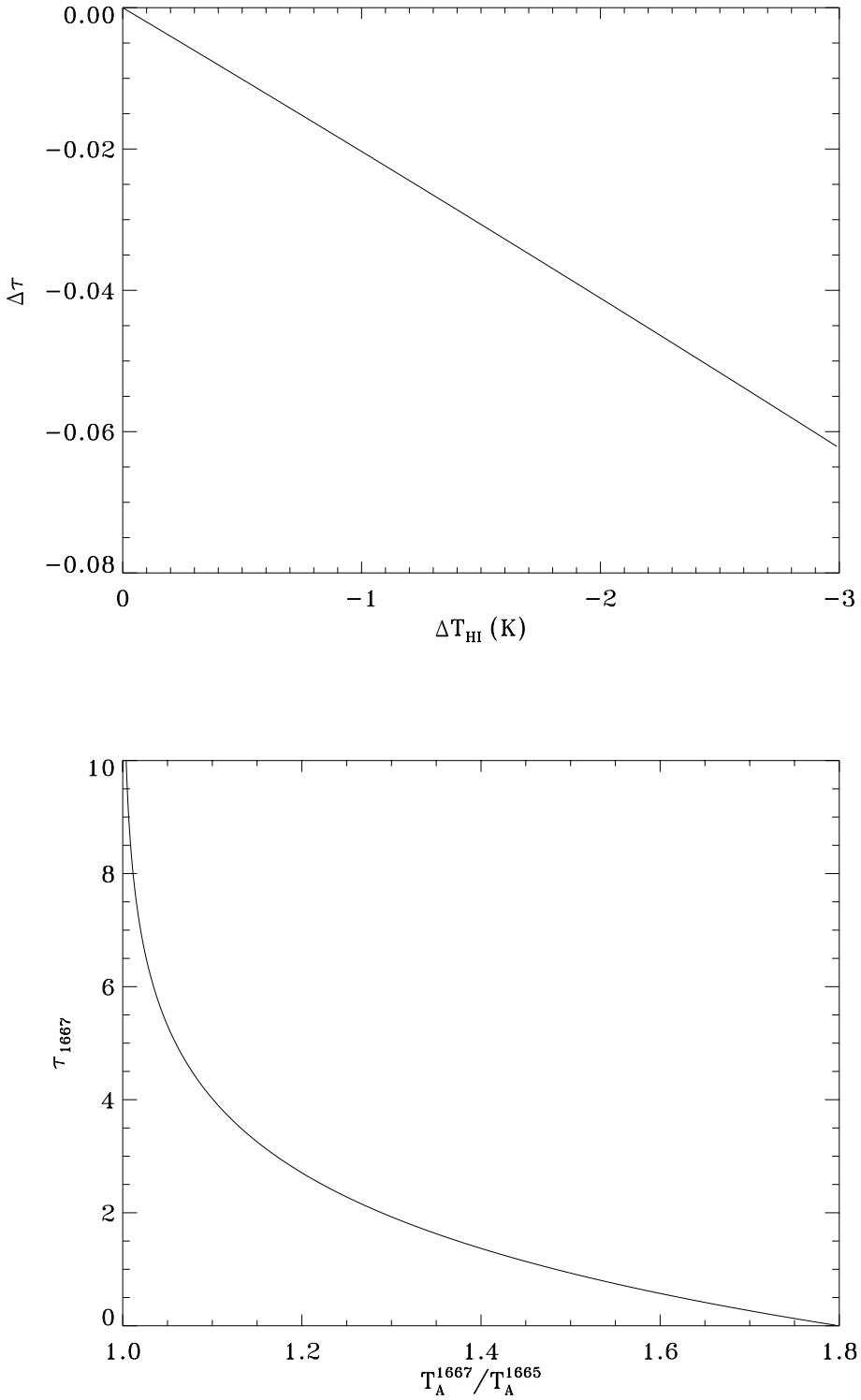

Fig. 6.— Upper panel: the uncertainties in derived optical depth of HINLA ($\Delta\tau$) caused by the fitting error of background HI emission (ΔT_{HI}). Lower panel: The relation between the ratio of antenna temperatures of the OH Λ doubling lines and the optical depth of the main line at 1667 MHz.

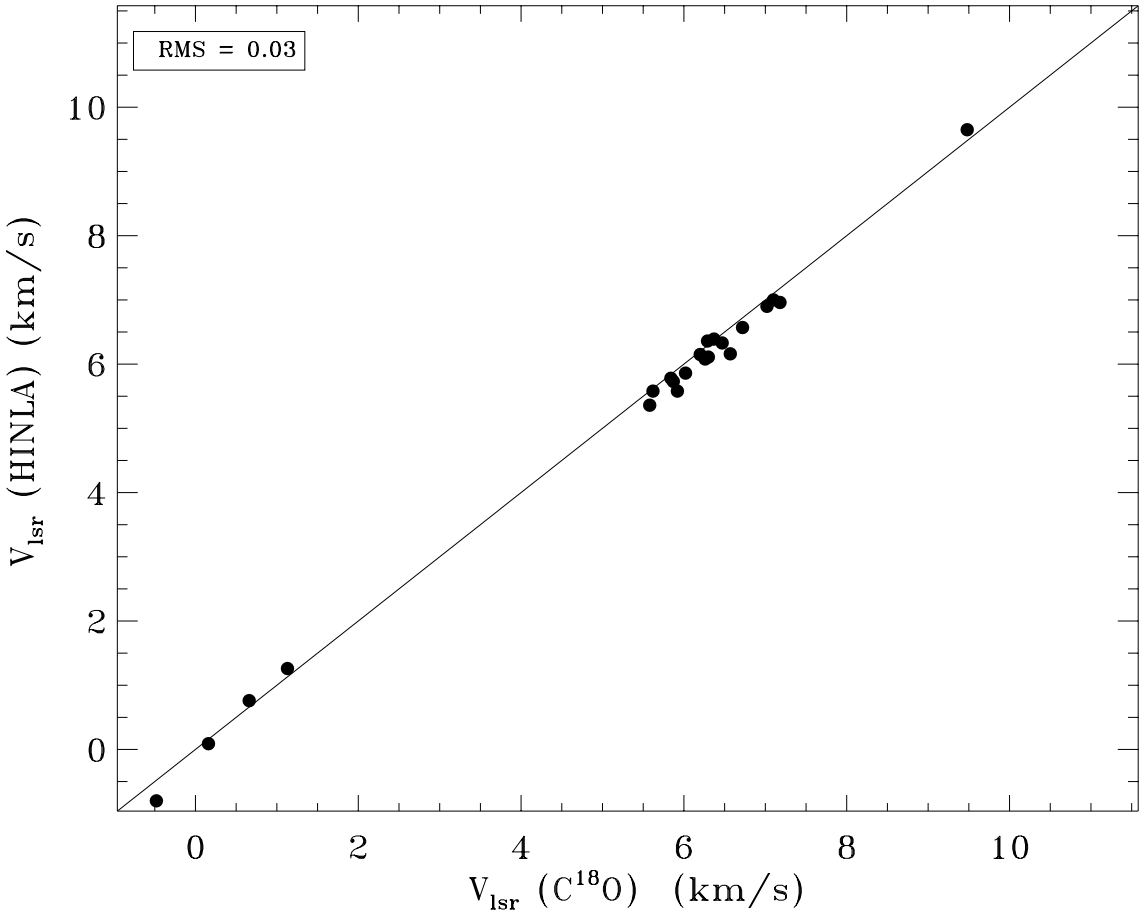

Fig. 7.— Comparison of the peak velocity of $C^{18}O$ with that of HINLA.

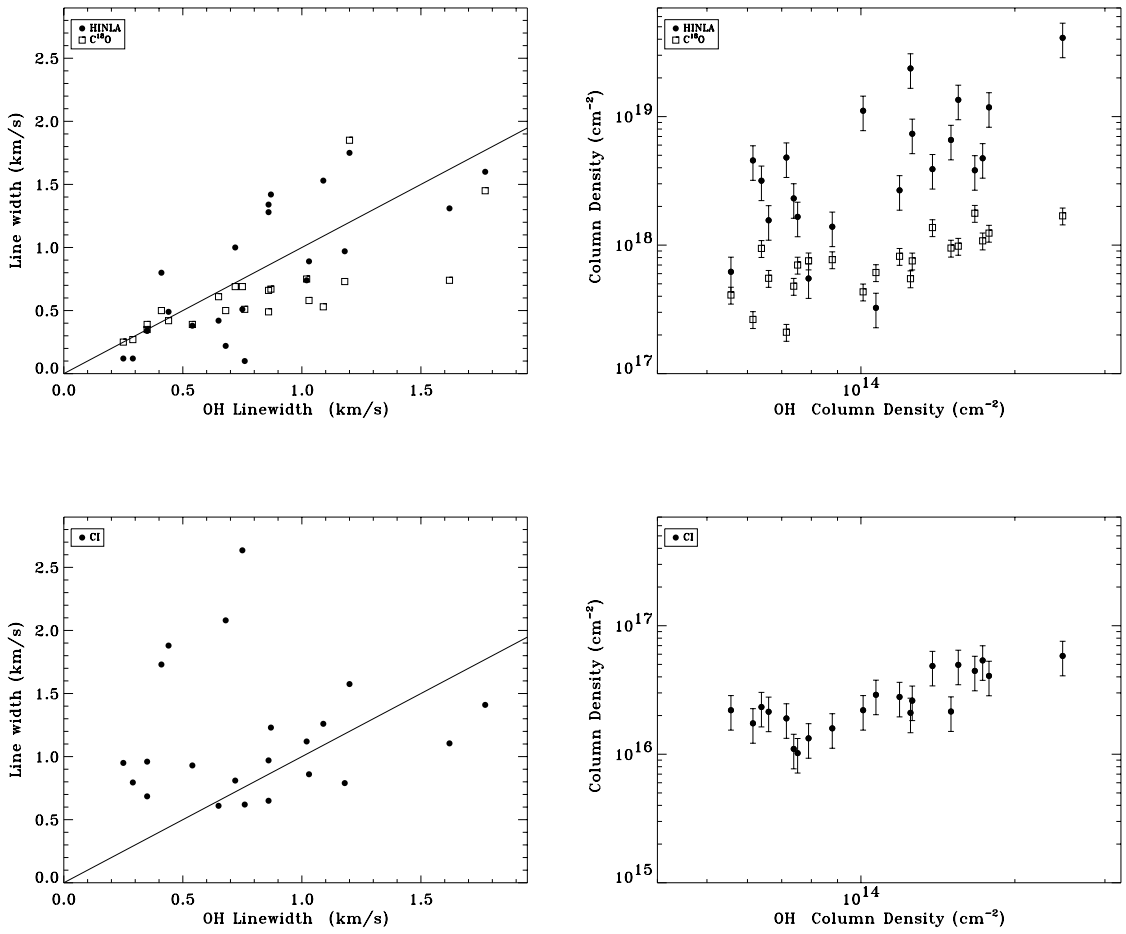

Fig. 8.— Left panels: nonthermal line width of OH, $C^{18}O$, HINLA and CI. Right panels: column densities of of OH, $C^{18}O$, HINLA and CI. In the upper right panel, the values of $C^{18}O$ column density have been multiplied by a factor of 10^3 in order to be plotted on the same scale. The straight lines in the left hand panels indicate equal line widths for the species observed and the OH, used as a reference. The HINLA and $C^{18}O$ emission exhibit essentially the same line width as the OH in a given cloud, while the CI line width is significantly larger than that of the OH.